Soluble P3HT-Grafted Graphene for Efficient Bilayer–Heterojunction Photovoltaic Devices

Dingshan Yu,[†] Yan Yang,[‡] Michael Durstock,[§,*] Jong-Beom Baek,[⊥] and Liming Dai[†,*]

[†]Department of Chemical Engineering, Case Western Reserve University, Cleveland, Ohio 44106, [‡]Department of Chemistry and Biochemistry, New Mexico State University, New Mexico 88003, [§]Materials and Manufacturing Directorate, Air Force Research Laboratory, RXBP, Wright-Patterson Air Force Base, Ohio 45433, and [⊥]Interdisciplinary School of Green Energy, Ulsan National Institute of Science and Technology (UNIST), 100, Banyeon, Ulsan, 689-798 South Korea

ABSTRACT CH_2OH-terminated regioregular poly(3-hexylthiophene) (P3HT) was chemically grafted onto carboxylic groups of graphene oxide (GO) *via* esterification reaction. The resultant P3HT-grafted GO sheets (G-P3HT) are soluble in common organic solvents, facilitating the structure/property characterization and the device fabrication by solution processing. The covalent linkage and the strong electronic interaction between the P3HT and graphene moieties in G-P3HT were confirmed by spectroscopic analyses and electrochemical measurements. A bilayer photovoltaic device based on the solution-cast G-P3HT/C_{60} heterostructures showed a 200% increase of the power conversion efficiency ($\eta = 0.61\%$) with respect to the P3HT/C_{60} counterpart under AM 1.5 illumination (100 mW/cm^2).

KEYWORDS: graphene · poly(3-hexylthiophene) · end-functionalization · solution processing · solar cells

The photovoltaic effect involves the generation of electrons and holes in a semiconductor device under illumination and the subsequent charge collection at opposite electrodes.[1−8] Photon absorption of organic optoelectronic materials often creates bound electron-hole pairs (*i.e.*, excitons). Charge collection, therefore, requires dissociation of the excitons, which occurs only at the heterojunction interface between semiconducting materials of different ionization potentials or electron affinities. Soluble conjugated polymers and fullerene have been widely used as electron donors (D) and acceptors (A) to enhance the charge separation.[1−5] The photoinduced charge transfer between the excited conducting polymer donor and C_{60} acceptor can occur very rapidly on a subpicosecond time scale with a quantum efficiency of close to unity for charge separation from donor to acceptor. Because the exciton diffusion range is typically at least a factor of 10 smaller than the optical absorption depth, the photoexcitations produced far from the interface recombine before diffusing to the heterojunction. In order to overcome this deficiency, bulk heterojunction photovoltaic cells based on interpenetrating networks consisting of a polymeric electron donor [*e.g.*, poly(3-hexylthiophene)] and a C_{60} derivative acceptor (typically, [6,6]-phenyl-C_{61}-butyric acid methyl ester, PCBM) have been developed.[1,6]

The bulk heterojunction concept has been widely used for polymer photovoltaic cells. Due to its high interfacial contact area between the donor and acceptor, the bulk heterojunction is more effective compared with a bilayer device structure. Miscibility between the electron acceptor and donor at the interface, either caused by a cosolvent effect or postfabrication diffusion, also creates problems in a bilayer device. Furthermore, the overall energy conversion efficiency of a bilayer device is diminished by the limited effective interfacial area available in the layer structure, and the photoexcitations produced far from the interface recombine before diffusing to the bilayer heterojunction. However, a bilayered device structure could be more favorable with respect to the bulk heterojunction for efficient charge transport since the separated charge carriers can easily transport to the opposite electrodes with a minimized recombination possibility.[7−9] In this regard, Wang et al.[9] reported that a P3HT/PCBM bilayer polymer solar cell with a concentration gradient showed an enhanced photocurrent density and power conversion efficiency compared to those of the bulk heterojunction photovoltaic cells under the same condition. On the other hand, the C_{60} layer in bilayer devices could provide an additional protection to the polymer layer from possible degradation caused by oxygen and humidity, thus improving the device stability.[10] More importantly, the bilayer structure allows the C_{60} layer to prevent

*Address correspondence to liming.dai@case.edu (L.D.), michael.durstock@wpafb.af.mil (M.D.).

Received for review May 20, 2010 and accepted September 01, 2010.

Published online September 10, 2010.
10.1021/nn101671t

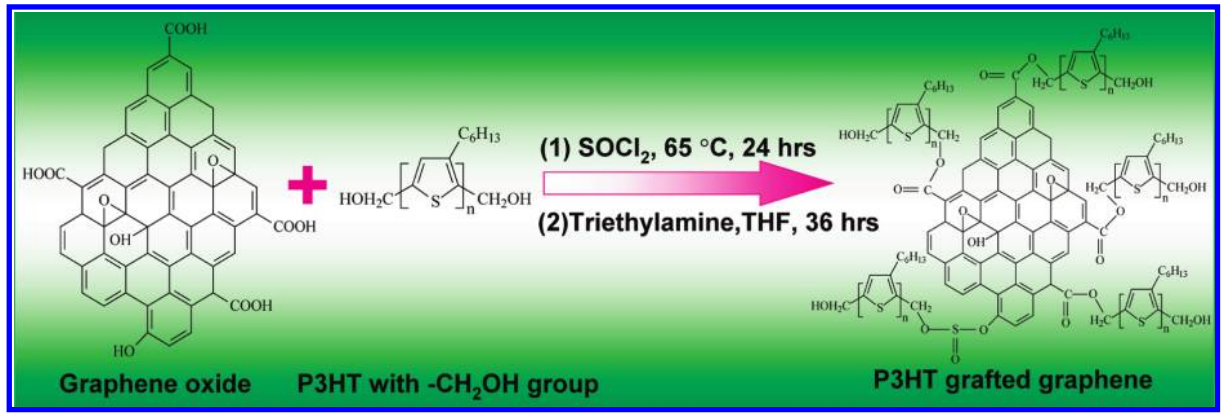

Figure 1. (a) Synthesis procedure for chemical grafting of CH_2OH-terminated P3HT chains onto graphene, which involves the $SOCl_2$ treatment of GO (step 1) and the esterification reaction between acyl-chloride functionalized GO and MeOH-terminated P3HT (step 2).

the polymer layer from direct contact with the cathode, reducing the recombination loss and eliminating any possible short circuit problem for polymer hybrid solar cells containing conducting additives (*e.g.*, carbon nanotubes, graphene sheets; see below). In this study, therefore, we focus on the bilayer structure to demonstrate potential applications of P3HT-grafted graphene (G-P3HT) in photovoltaic devices.

As can be seen from above discussion, efficient photovoltaic cells should involve materials with a relatively high charge mobility and large D−A interface for efficient excition dissociation and transport.[5,11] Along with certain inorganic nanoparticles (*e.g.*, CdSe,[12,13] CdTe,[5] and ZnO[14,15] nanocrystals), carbon nanotubes (CNTs) have recently been used in bilayer and bulk heterojunction polymer photovoltaic devices to provide the large surface/interface area as well as good electronic properties for enhanced charge separation and transport.[16−20] However, significant improvement in the overall device performance has not been achieved for CNT-based polymer photovoltaic cells due largely to technical difficulties in dispersing CNTs homogenously in the polymer matrix without any short-circuit problem, particularly in the bulk heterojunction photovoltaic devices.

As the building blocks for CNTs and other carbon nanomaterials, the two-dimensional (2-D) single atomic carbon sheets of graphene show remarkable electronic, thermal, and mechanical properties attractive for a variety of potential device applications.[21−25] Of particular interest, graphene shows the highest room-temperature mobility for electron and hole transport among all known carbon nanomaterials.[25] Compared with CNTs, the one-atom thickness and 2-D carbon network of graphene lead to a much higher specific surface area (hence, a larger interface in a polymer matrix) and a reduced through-thickness short circuit for the photovoltaic active layer even in a bulk heterojunction device.[22,26] Therefore, the combination of graphene sheets with conjugated polymers is of great promise for polymer-based photovoltaic cells. However, the potential application of graphene sheets in polymer photovoltaic devices has been precluded by their poor solubility, which makes the graphene dispersion and device fabrication very difficult, if not impossible, by the traditional solution processing methods (*e.g.*, spin- or blade-coating). Fortunately, the presence of oxygen-containing functional groups (*e.g.*, −OH and −COOH) in graphene oxide (GO) could not only impart solubility for large-scale film formation through solution processes (*e.g.*, spin-casting and layer-by-layer self-assembling)[27] but also facilitate chemical functionalization of graphene for various applications.[28] Although some efforts have been made toward polymer functionalization of GO sheets, no attempt has been reported for conjugated polymer chains.[29]

In this study, we have chemically grafted CH_2OH-terminated regioregular poly(3-hexylthiophene) (P3HT) mainly onto carboxylic groups of GO sheets *via* esterification reaction. The resultant P3HT-grafted GO sheets (G-P3HT) are soluble in common organic solvents, facilitating the structure/property characterization and device fabrication by solution processing. In particular, we have found that a bilayer photovoltaic device based on the solution-cast G-P3HT heterostructure with thermally evaporated C_{60} showed an up to 200% increase in the power conversion efficiency compared to its P3HT/C_{60} counterpart under AM 1.5 illumination (100 mW/cm^2). The resultant power conversion efficiency of 0.61% indicates that the G-P3HT/C_{60} bilayer photovoltaic device is also more efficient than its counterpart with electron donors based on P3HT with and without doping by CNT or inorganic nanocrystals, such as CdTe tetrapods.[5,17−19]

RESULTS AND DISCUSSION

GO was prepared according to a modified Hummers method.[30] Individual GO sheets thus produced with a thickness of ~1.3 nm and size distribution in the range of 0.2−2 μm are shown in Figure S1 of the Supporting Information. End functionalization of P3HT was carried out according to the reported procedure to yield

−CH_2OH end groups[31] (Scheme S1, Supporting Information). As for the preparation of the P3HT grafted graphene, GO was first reacted with $SOCl_2$ to obtain acyl-chloride functionalized GO. Then, a condensation reaction between the CH_2OH-terminated P3HT and the acyl-chloride functionalized GO was performed to yield the G-P3HT (Figure 1). The final G-P3HT product can be easily redispersed in common organic solvents, such as THF, chloroform, and toluene, under sonication.

Figure 2 shows X-ray photoelectron spectroscopy (XPS) spectra of GO before and after grafting with the CH_2OH-terminated P3HT chains. While Figure 2a shows only the C and O peaks for GO, the corresponding XPS spectrum for the purified G-P3HT in Figure 2b reveals the presence of carbon, oxygen, and sulfur, arising from the P3HT chains and graphene sheets. Figure 2c reproduces the high-resolution C1s spectrum for GO, which exhibits the presence of C−C (284.5), C−O (286.4), C═O (288.0) and COOH (289.0 eV) groups. Upon polymer grafting (Figure 2d), the intensities of the C═O and COOH peaks decreased dramatically due to the formation of ester linkages between the COOH groups of GO and the hydroxyl groups of the CH_2OH-terminated P3HT. The presence of the ester linkages in G-P3HT is also evidenced by the C═O and C−O peaks at 288.0 and 286.5 eV in Figure 2d, though the contribution from some unreacted functional groups in the GO cannot be ruled out. While the esterification reaction between the acyl-chloride functionalized GO and CH_2OH-terminated P3HT significantly reduced the COOH component of GO, the significant decrease of the C−O component in Figure 2c suggests possible activation of the −OH groups of GO by thionyl chloride and subsequent grafting of the CH_2OH-terminated P3HT onto the activated −OH group of GO by the formation of O−S(O)−O linkage (Figure 1).[32]

The ester linkage between P3HT and graphene in G-P3HT was also confirmed by ^{1}H NMR measurements (Figure S2−S4, Supporting Information) and further checked by Fourier transform infrared (FTIR) spectroscopy. As shown in Figure 3 (solid line), the pure GO shows the peaks of OH (O−H stretching vibrations) at 3431, C═O (carboxylic acid and carbonyl moieties) at 1731, and C−C (skeletal vibration of graphitic domains) at 1627 cm^{-1}, along with the broad band over 1000−1400 cm^{-1} arising from the C−OH (1227) and C−O (1075) stretching vibrations.[33] For the G-P3HT (Figure 3, dash line), the bands at 1726 and 1242 cm^{-1} can be attributed to the C═O stretching and the C−O stretching of the ester groups, respectively, confirming the formation of covalent bonding between graphene and P3HT.[34] Besides, the presence of P3HT is confirmed by the appearance of three absorption bands at 2960, 2925, and 2855 cm^{-1} associated with aliphatic C−H stretching of P3HT and the 821 cm^{-1} band corresponding to aromatic C−H bending of P3HT.[35]

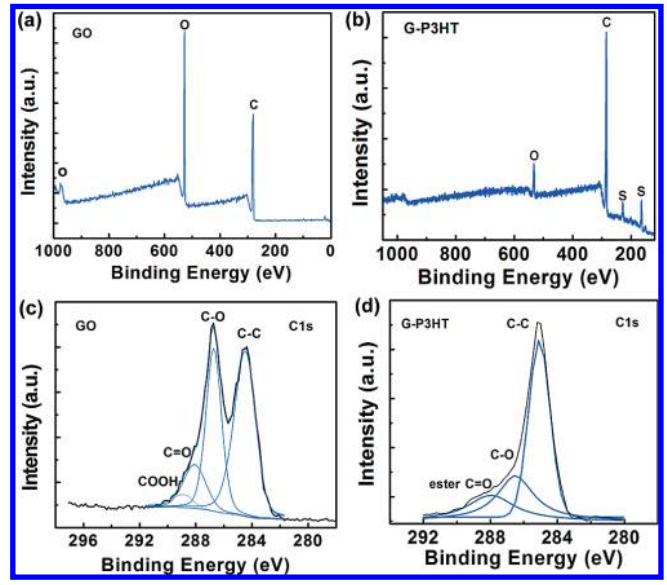

Figure 2. XPS spectra of GO and G-P3HT. (a, b) Survey spectra and (c, d) high-resolution C1s spectra.

Figure 4a shows the normalized absorption spectra of pure P3HT and G-P3HT in chloroform solution. A strong absorption band at 446 nm attributable to the $\pi-\pi^*$ transition[36] was seen for pure P3HT, which red-shifted to about 458 nm upon grafting onto graphene in G-P3HT. However, the simple mixture of P3HT and graphene in the same solvent did not cause any significant change in the P3HT absorption band (Figure S5, Supporting Information). These results indicate that there exists a strong interaction between P3HT and graphene in G-P3HT. Such specific interaction probably increases the electron delocalization along the polymer chain, thus leading to the observed red-shift of the optical absorption peak.[18] The UV−vis absorption spectra for thin films of pure P3HT and G-P3HT are also shown in Figure 4a. As expected, the P3HT thin film showed a significant red-shift of the $\pi-\pi^*$ absorption up to ~512 nm from the corresponding solution absorption at 446 nm due, most probably, to the strong interchain interaction in the regioregular P3HT thin

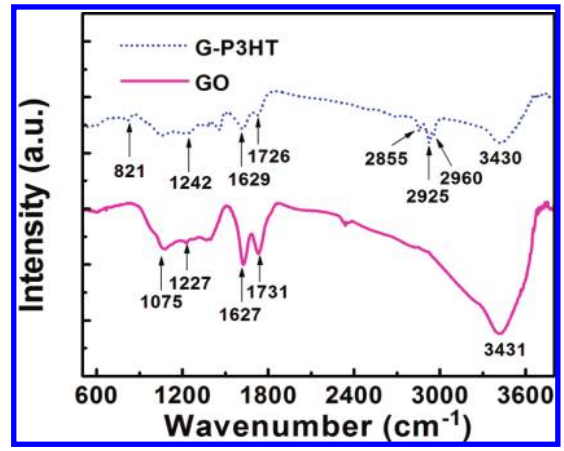

Figure 3. FTIR spectra of GO before and after grafting with P3HT chains.

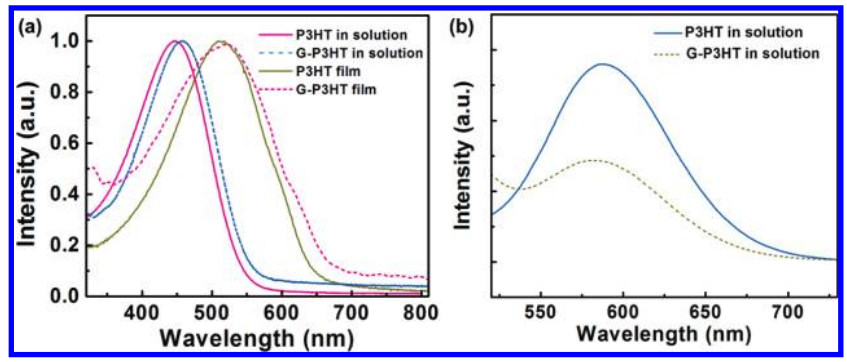

Figure 4. (a) UV−vis absorption spectra of pure P3HT and G-P3HT (solid and dash lines, respectively) in $CHCl_3$ solution at 1 mg/mL and of solid thin film prepared by spin-coating on quartz plates. (b) PL spectra of pure P3HT and G-P3HT (solid and dash lines, respectively) in $CHCl_3$ solution at 1 mg/mL and λ_{ex} = 450 nm.

film. The absorption band of the G-P3HT film also showed a strong red-shift up to ~522 nm from the corresponding solution absorption at 458 nm. The graphene-induced enhancement in electron delocalization along the chemically grafted P3HT chains was also observed in the G-P3HT film, as evidenced by about 10 nm red-shift in the absorption band of the G-P3HT film with respect to that of the P3HT film. The observed red-shifts for the $\pi-\pi^*$ absorption band of G-P3HT in both the solution and the solid state upon being grafted onto graphene indicate an enhanced electron delocalization through charge transfer with the chemically conjugated graphene sheet to reduce the band gap energy; an advantage for the photovoltaic application.[37,38] As can be seen in Figure 1, one end of the P3HT chain in the $HOH_2C-P3HT-CH_2OH$ will be grafted onto one graphene sheet, while the other end of the same polymer chain may attach to the same or to another graphene sheet to form a continuous network structure. This should also facilitate the charge transport in photovoltaic cells. Figure 4b shows photoluminescence (PL) spectra of P3HT and G-P3HT in chloroform solution at an excitation wavelength of 450 nm. As can be seen, the pure P3HT shows a strong emission band over 550−650 nm, which was remarkably reduced for G-P3HT due to the PL quenching effect caused by graphene.[22] This is an additional advantage for using the G-P3HT in photovoltaic cells.

PL lifetime measurements can provide another evidence for the charge-transfer interaction between P3HT and the graphene in G-P3HT. If the observed PL quenching for P3HT in the G-P3HT results from the charge-transfer interaction with graphene, then the chemical grafting of P3HT chains onto the graphene should accelerate the decay of the P3HT emission. To investigate charge-transfer interaction, we performed time-resolved emission studies by using an excitation wavelength of 410 nm. The PL lifetime was calculated by fitting data to a single exponential decay function.[39] The PL lifetime profiles for the pristine P3HT and G-P3HT are given in Figure 5, which, as expected, shows a PL lifetime of 507 ps for the pristine P3HT in $CHCl_3$ and a much shorter PL lifetime of 380 ps for the G-P3HT. Therefore, the charge-transfer interaction indeed occurred between the P3HT and the graphene in G-P3HT, providing a new nonradiative decay pathway for photogenerated excitons in the G-P3HT. Furthermore, G-P3HT also shows a relatively fast decay time compared with the simple mixture of P3HT and graphene (*i.e.*, G/P3HT) having a PL lifetime of 476 ps (Figure 5). As a result, the chemical linkage between the P3HT and graphene could facilitate the exciton dissociation for the solar cell application.

To demonstrate the potential application of the G-P3HT in photovoltaic cells, we carried out cyclic voltammetry (CV) measurements of pure P3HT and G-P3HT for determining their band gap energies. The CV of both P3HT and G-P3HT revealed well-defined oxidation and reduction peaks (Figure S6, Supporting Information). From the onset of oxidation (E_{ox}) and reduction (E_{red}) potentials, we can calculate the highest occupied and lowest unoccupied molecular orbitals (HOMO and LUMO, respectively) energy levels as well as the energy gaps (E_g) of the polymers, according to the previously reported method (see experimental methods).[40] The obtained electrochemical data, together with the optical absorption data are summarized in Table 1. As can be seen, G-P3HT showed a lower HOMO level and a narrower band gap than that of P3HT. The relatively lower band gap observed for G-P3HT probably resulted from the above-mentioned charge-transfer interaction between the graphene sheets and end-anchored P3HT chains.[41]

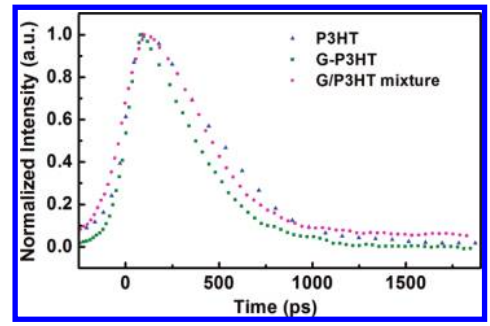

Figure 5. Time-resolved photoluminescence spectra of the pristine P3HT (1 mg/mL), G-P3HT (1 mg/mL), and G/P3HT mixture (1 mg/mL) in $CHCl_3$.

TABLE 1. Optical and electrochemical data of P3HT and G-P3HT

	UV−vis absorption						cyclic voltammetry		
	$CHCl_3$ solution			solid films			E_{ox} (V)	E_{red} (V)	
	λ_{max} (nm)	λ_{onset} (nm)	E_g (eV)	λ_{max} (nm)	λ_{onset} (nm)	E_g (eV)	HOMO (eV)	LUMO (eV)	E_g (eV)
P3HT	446	545	2.28	512	648	1.91	0.89/−5.29	−1.01/−3.39	1.90
G-P3HT	458	557	2.23	522	666	1.85	0.99/−5.39	−0.84/−3.56	1.83

As schematically shown in Figure 6a, polymer photovoltaic cells with the structure of ITO/PEDOT:PSS(30 nm)/G-P3HT or P3HT(60 nm)/C_{60}(45 nm)/Al(100 nm) were fabricated. A postfabrication annealing of the G-P3HT active layer was conducted at 160 °C for 20 min under N_2, which should not only improve the morphology of the P3HT matrix[42] but more importantly remove the residual functional groups in the graphene sheet to increase the conjugation length for enhancing the charge transport mobility.[22] Figure 6b gives the energy level diagram for the G-P3HT/C_{60} device, while Figure 6c shows the current−voltage (J−V) curves for both the G-P3HT/C_{60} and P3HT/C_{60} photovoltaic cells. As expected, no short circuit current (J_{sc}) was observed for either the P3HT or G-P3HT-based devices in dark. Upon 100 mW/cm^2 (AM 1.5 G) illumination, however, an open-circuit voltage (V_{oc}) of 0.43 V, short-circuit current density (J_{sc}) of 3.5 mA cm^{-2}, fill factor (*FF*) of 0.41, and overall power conversion efficiency (η) of 0.61% were obtained for the G-P3HT/C_{60} device. In contrast, the reference photovoltaic cell based on P3HT/C_{60} showed a much lower V_{oc} (0.23 V), J_{sc} (1.9 mA cm^{-2}), and η (0.20%) but a slightly higher *FF* (0.45). Therefore, the photovoltaic cell based on G-P3HT/C_{60} clearly outperformed its counterpart based on P3HT/C_{60}. While the increased J_{sc} for the photovoltaic device based on G-P3HT can be attributed to the enhanced charge transport/collection associated with the graphene sheets, the increased V_{oc} is not inconsistent with the reduced HOMO level of the P3HT upon end-anchoring onto the graphene sheet, as the V_{oc} for a bulk-heterojunction solar cell normally depends on the energy difference between the LUMO level of the electron acceptor and the HOMO level of the electron donor.[22] Consequently, significantly improved device performance with a remarkable increase in the power conversion efficiency up to 200% was repeatedly obtained for the G-P3HT devices with respect to the P3HT counterpart.

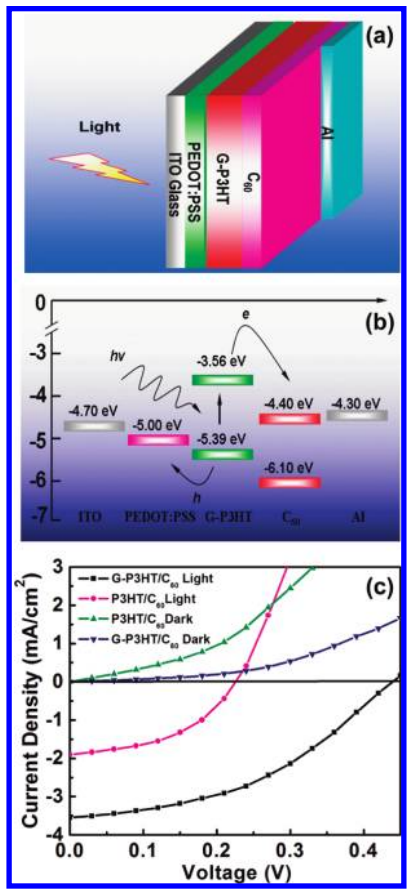

Figure 6. (a) Schematic and (b) energy level diagram of a ITO/PEDOT: PSS/G-P3HT/C_{60}/Al photovoltaic device. (c) Current−voltage characteristics of the photovoltaic devices using P3HT/C_{60} or G-P3HT/C_{60} as the active layer.

Table 2 summarizes typical device performance for about 10 bilayer photovoltaic cells investigated in this study, including the reference devices fabricated in the same manner with identical device parameters by using the mixture of graphene (2 wt %) and P3HT/C_{60} as the active layer. In this case, it was difficult to yield a homogeneous film by directly blending graphene with P3HT due to the aggregation of graphene in the polymer matrix. The graphene aggregation often has a deleterious effect on the charge separation/transport. Hence, the overall device efficiency was not remarkably improved (0.18%, Table 2), although the V_{oc} exhibited an increase relative to that of the P3HT/C_{60} device (I−V curve, Figure S7, Supporting Information). Therefore, the device based on G-P3HT/C_{60} showed the best overall device performance among all of the different type photovoltaic devices studied in the present work. Although the obtained power conversion efficiency of 0.61% is still moderate, it is significant for bilayer devices and already

TABLE 2. Device Performances of Several Donors/C_{60} Heterojunction Devices

	V_{oc} (V)	J_{sc} (mA/cm^2)	*FF*	η (%)
P3HT	0.23	1.9	0.45	0.20
G-P3HT	0.43	3.5	0.41	0.61
G/P3HT mixture	0.27	1.8	0.38	0.18

considerably higher than those of CNT or inorganic nanocrystal (CdTe)-doped P3HT (or P3OT)/C_{60} bilayer heterojunction solar cells[5,17−19] and even better than that of a CNT/P3HT/C_{60} bulk heterojunction solar cell.[20] Furthermore, the relatively low fill factor for the G-P3HT device indicates considerable room for further improvement in the device performance.

CONCLUSION

In summary, regioregular poly(3-hexylthiophene) (P3HT) chains have been covalently grafted onto graphene sheets *via* esterification between the carboxylic groups in GO and CH_2OH-terminated P3HT. The resultant P3HT-grafted GO sheets (G-P3HT) possess good solubility in common organic solvents (*e.g.*, THF), facilitating the structure/property characterization and device fabrication by solution processing.

Detailed spectroscopic and electrochemical measurements indicated that chemical grafting of P3HT onto graphene induced a strong electronic interaction, leading to an enhanced electron delocalization and a slightly reduced band gap energy for the graphene-bound P3HT, with respect to pure P3HT. Bilayer photovoltaic devices based on the G-P3HT/C_{60} heterostructures showed a higher short circuit current and open circuit voltage with a 200% increase in the power conversion efficiency compared to its pure P3HT/C_{60} counterpart. Therefore, the organic soluble G-P3HT holds great promise for a wide range of potential applications in optoelectronic devices.

METHODS

Preparation of GO Nanosheets. GO sheets were prepared from exfoliation of graphite according to a modified Hummers method.[30] Briefly, commercially obtained graphite powder (Aldrich) was vigorously stirred for five days in a mixture of H_2SO_4 (98%), $NaNO_3$, and $KMnO_4$. After completion of the reaction, the mixture was washed with 5% H_2SO_4 in water. Consequently, 30% H_2O_2 was added to the reaction vessel, and the mixture was stirred for 2 h at room temperature. The GO was filtered and washed three times with 1 M HCl and three times with DI water. The GO can be separated and dried into a brown powder form. The AFM image of the obtained GO sheets is shown in Figure S1, Supporting Information.

Preparation of P3HT-Grafted Graphene. End-functionalized regioregular P3HT with methylene hydroxy groups was synthesized by the previously reported method.[31] The presence of the methylene hydroxy groups at ends was confirmed by NMR results (see Figures S2−S4, Supporting Information). In a typical experiment for the synthesis of the P3HT-grafted graphene, dried GO sample (25 mg) was refluxed in thionyl chloride (25 mL) for 24 h, followed by the removal of excess thionyl chloride under vacuum. CH_2OH-terminated P3HT (100 mg) in 30 mL THF was then added through a syringe to the thionyl chloride treated GO under stirring, followed by the addition of triethylamine (15 mL) in nitrogen atmosphere. After sonication for 2 h, the reaction mixture was vigorously stirred for 36 h, leading to a dark suspension. The solid in the suspension was removed by centrifuging at 5000 rpm for 10 min, and the solvent in the clear solution thus prepared was partially removed by evaporation. It was further purified by precipitating in methanol, filtering, and solvent-washing thoroughly to remove the excess triethylamine. The final product was dried in vacuum oven for 24 h at 60 °C.

Microscopic and Spectroscopic Characterization. The surface topology of GO was examined using an atomic force microscopy microscope (AFM, Micro 40, and Pacific Technology) in the tapping mode under ambient atmosphere. The surface chemistry was analyzed using a VG Micro Tech ESCA 2000 X-ray photoelectron spectrometer (XPS). Fourier transform infrared (FTIR) spectra were recorded on a Perkin-Elmer FTIR spectrometer (Spectrum ONE). NMR measurements were performed in $CDCl_3$ on a Bruker 300 MHz NMR spectrometer. Thermogravimetric analyses (TGA) were made on a TA Q50 instrument under N_2 atmosphere with a heating rate of 20 °C/min. UV−vis absorption spectra were recorded on a Perkin-Elmer Lambda 900 UV−vis-NIR spectrophotometer. Photoluminescence (PL) spectroscopy was done with a LS55 spectrometer (Perkin-Elmer) at an excitation wavelength of 450 nm. Time-resolved photoluminescence spectroscopy was performed with a time-correlated single photon counting spectrometer. Output of a mode-locked Ti:sapphire laser running at 820 nm was doubled to generate excitation pulses at 410 nm.

Electrochemical Measurements. To investigate the electrochemical properties of P3HT before and after being grafted onto graphene and to estimate their HOMO and LUMO energy levels, cyclic voltammetry (CV) was carried out by using a standard three-electrode system, which consists of a glassy carbon disk as the working electrode, a platinum wire as the counter electrode, and a silver wire as the reference electrode. The polymer electrode was prepared by drop-casting of a polymer solution onto the glassy carbon electrode. CV was recorded in acetonitrile containing 0.1 M tetrabutylammonium hexafluorophosphate ($TBAPF_6$, Aldrich) as the supporting electrolyte. Before each measurement, the electrochemical cell was purged with high-purity argon gas for 15 min. The HOMO and LUMO energy levels in eV as well as the electrochemical energy gap (E_g in eV) of the samples were calculated according to the following equations:[37]

$$E_{HOMO} = -e(E_{ox} + 4.4) \quad (1)$$

$$E_{LUMO} = -e(E_{red} + 4.4) \quad (2)$$

$$E_g = e(E_{ox} - E_{red}) \quad (3)$$

where E_{ox} and E_{red} are the onset of oxidation and reduction potential, respectively.

Fabrication and Characterization of Photovoltaic Devices. Indium tin oxide (ITO, 25 Ω/sq) coated glass plates were used as the substrate for the device fabrication. The substrates were cleaned by consecutive sonication in detergent (MICRO-90), deionized water, isopropyl alcohol, and acetone in an ultrasonic bath (VWR model 75 D), followed by a 10 min UV−ozone treatment. Poly(3,4-ethylenedioxythiophene):poly(styrenesulfonate) (PEDOT: PSS) (Bayton P, ~30 nm in thickness) was spin coated onto the clean substrates, which were subsequently dried at 120 °C for 10 min to remove residual water. Photovoltaic devices were then fabricated in a glovebox under nitrogen atmosphere by spin coating a G-P3HT thin film (60 nm) from its chlorobenzene solution (10 mg/mL), followed by annealing at 160 °C for 20 min. Thereafter, a thin layer of C_{60} (45 nm) was vacuum evaporated onto the G-P3HT surface, followed by vacuum evaporation of Al (100 nm) onto the C_{60} layer through a shadow mask to define an active area of 6 mm^2 for each device. The current−voltage (J−V) curves of the photovoltaic devices were recorded on a Keithly 236 source-measurement unit. The photocurrent was measured under simulated AM1.5G irradiation (100 mW/cm^2), using a xenon lamp-based solar simulator (XPS-400, Solar Light Co.). All devices were fabricated and tested in oxygen and moisture-free environment under nitrogen inside the glovebox. For comparison, bilayer solar cells based on pure P3HT/C_{60} and on P3HT mixed with graphene (2 wt %) /C_{60} were also fabricated and investigated under the same condition.

Acknowledgment. The authors thank the support from AFOSR (FA9550-09-1-0331) and WCU Project through UNIST from the Ministry of Education, Science, and Technology in Korea.

Supporting Information Available: AFM image of GO nanosheets, ^{1}H NMR spectra of the regioregular P3HT with −CHO or $-CH_2OH$ end groups and the P3HT grafted graphene, absorption spectra of the mixture of graphene and P3HT in chloroform, and the *J*−*V* curve from a bilayer solar cell based on the mixture of graphene and P3HT/C_{60} are seen in Figures S1−S7. This information is available free of charge *via* the Internet at http://pubs.acs.org.

REFERENCES AND NOTES

1. Heeger, A. J. Semiconducting and Metallic Polymers: the Fourth Generation of Polymeric Materials. *Angew. Chem., Int. Ed.* **2001**, *40*, 2591–2611.
2. Tompson, B. C.; Frechet, J. M. Polymer-Fullerene Composite Solar Cells. *Angew. Chem., Int. Ed.* **2008**, *47*, 58–77.
3. Kim, Y.; Shin, M.; Lee, I.; Kim, H.; Heutz, S. Multilayer Organic Solar Cells with Wet-processed Polymeric Bulk Heterojunction Film and Dry-processed Small Molecule Films. *Appl. Phys. Lett.* **2008**, *92*, 093306.
4. Kim, K.; Liu, J.; Carroll, D. L. Thermal Diffusion Processes in Bulk Heterojunction Formation for Poly-3-hexylthiophene/C_{60} Single Heterojunction Photovoltaics. *Appl. Phys. Lett.* **2006**, *88*, 181911.
5. Li, Y.; Mastria, R; Li, K.; Fiore, A.; Wang, Y.; Cingolani, R.; Manna, L.; Gigli, G. Improved Photovoltaic Performance of Bilayer Heterojunction Photovoltaic Cells by Triplet Materials and Tetrapod-shaped Colloidal Nanocrystals Doping. *Appl. Phys. Lett.* **2009**, *95*, 043101.
6. Sun, S. S.; Sariciftci, N. S. *Organic Photovoltaics: Mechanisms, Materials and Devices*; CRC Press: Boca Raton, FL, 2005.
7. Sun, Q.; Park, K. S.; Dai, L. Liquid Crystalline Polymers for Efficient Bilayer-Bulk-Heterojunction Solar Cells. *J. Phys. Chem. C* **2009**, *113*, 7892–7897.
8. Sun, Q.; Dai, L.; Zhou, X.; Li, L.; Li, Q. Bilayer- and Bulk-heterojunction Solar Cells using Liquid Crystalline Porphyrins as Donors by Solution Processing. *Appl. Phys. Lett.* **2007**, *91*, 253505.
9. Wang, D. H.; Lee, H. K; Choi, D.; Park, J. H.; Park, O. Solution-processable Polymer Solar Cells from a Poly(3-hexylthiophene)/[6,6]-phenyl C61-butyric Acidmethyl Ester Concentration Graded Bilayers. *Appl. Phys. Lett.* **2009**, *95*, 043505.
10. Li, Y.; Mastria, R.; Fiore, A.; Nobile, C.; Yin, L.; Biasiucci, M.; Cheng, G.; Cucolo, A.; Cingolani, R.; Manna, L.; et al. Improved Photovoltaic Performance of Heterostructured Tetrapod-Shaped CdSe/CdTe Nanocrystals Using C_{60} Interlayer. *Adv. Mater.* **2009**, *21*, 4461–4466.
11. Peumans, P.; Uchida, S.; Forrest, S. R. Efficient Bulk Heterojunction Photovoltaic Cells using Small-molecular-weight Organic Thin Films. *Nature* **2003**, *425*, 158–162.
12. Huynh, W. U.; Dittmer, J. J.; Alivisatos, A. P. Hybrid Nanorod-polymer Solar Cells. *Science* **2002**, *295*, 2425–2427.
13. Liu, J. S.; Tanaka, T.; Sivula, K.; Alivisatos, A. P.; Frechet, J. M. J. Employing End-Functional Polythiophene To Control the Morphology of Nanocrystal-Polymer Composites in Hybrid Solar Cells. *J. Am. Chem. Soc.* **2004**, *126*, 6550–6551.
14. Law, M.; Greene, L. E.; Johnson, J. C.; Saykally, R.; Yang, P. Nanowire Dye-sensitized Solar Cells. *Nat. Mater.* **2005**, *4*, 455–459.
15. Oosterhout, S. D.; Wienk, M. M.; van Bavel, S. S.; Thiedmann, R.; Koster, L. J. A.; Gilot, J.; Loos, J.; Schmidt, V.; Janssen, R. A. J. The Effect of Three-dimensional Morphology on the Efficiency of Hybrid Polymer Solar Cells. *Nat. Mater.* **2009**, *8*, 818–824.
16. Reyes-Reyesa, M.; Lopez-Sandovalb, R.; Liu, J.; Carrollc, D. L. Bulk Heterojunction Organic Photovoltaic Based on Polythiophene-polyelectrolyte Carbon Nanotube Composites. *Sol. Energy Mater. Sol. Cells* **2007**, *91*, 1478–1482.
17. Pradhan, B.; Batabyal, S. K.; Pala, A. J. Functionalized Carbon Nanotubes in Donor/Acceptor-type Photovoltaic Devices. *Appl. Phys. Lett.* **2006**, *88*, 093106.
18. Arranz-Andres, J.; Blau, M. J. Enhanced Device Performance Using Different Carbon Nanotube Types in Polymer Photovoltaic Devices. *Carbon* **2008**, *46*, 2067–2075.
19. Somani, P. R.; Somani, S. P.; Flahaut, E.; Umeno, M. Improving Photovoltaic Response of Poly(3-octylthiophene)/n-Si Heterojunction by Incorporating Double Walled Carbon Nanotubes. *Nanotechnology* **2007**, *18*, 185708–185802.
20. Li, C.; Chen, Y.; Wang, Y.; Iqbal, Z.; Chhowalla, M.; Mitra, S. A Fullerene-Single Wall Carbon Nanotube Complex for Polymer Bulk Heterojunction Photovoltaic Cells. *J. Mater. Chem.* **2007**, *17*, 2406–2411.
21. Wang, X.; Zhi, L. J.; Mullen, K. Transparent, Conductive Graphene Electrodes for Dye-sensitized Solar Cells. *Nano Lett.* **2008**, *8*, 323–327.
22. Liu, Z.; Liu, Q.; Huang, Y.; Ma, Y.; Yin, S.; Zhang, Chen, Y.; Sun, W.; Chen, Y. Organic Photovoltaic Devices Based on a Novel Acceptor Material: Graphene. *Adv. Mater.* **2008**, *20*, 3924–3930.
23. Yu, D.; Dai, L. Voltage-induced Incandescent Light Emission from Large-area Graphene Films. *Appl. Phys. Lett.* **2010**, *96*, 143107.
24. Qu, L.; Liu, Y.; Baek, J.; Dai, L. Nitrogen-Doped Graphene as Efficient Metal-Free Electrocatalyst for Oxygen Reduction in Fuel Cell. *ACS Nano* **2010**, *4*, 1321–1326.
25. Eda, G.; Chhowalla, M. Graphene-based Composite Thin Films for Electronics. *Nano Lett.* **2009**, *9*, 814–818.
26. Yang, N.; Zhai, J.; Wang, D.; Chen, Y.; Jiang, L. Two-dimensional Graphene Bridges Enhanced Photoinduced Charge Transport in Dye-Sensitized Solar Cells. *ACS Nano* **2010**, *4*, 887–894.
27. Yu, D.; Dai, L. Self-Assembled Graphene/Carbon Nanotube Hybrid Films for Supercapacitors. *J. Phys. Chem. Lett.* **2010**, *1*, 467–470.
28. Liu, Y.; Yu, D.; Zeng, C.; Miao, Z.; Dai., L. Biocompatible Graphene-oxide-based Glucose Biosensors. *Langmuir* **2010**, *29*, 6158–6160.
29. Salavagione, H. J.; Gomez, M. A.; Martnez, G. Polymeric Modification of Graphene through Esterification of Graphite Oxide and Poly(vinylalcohol). *Macromolecules* **2009**, *42*, 6331–6334.
30. Becerril, H. A.; Mao, J.; Liu, Z.; Stoltenberg, R. M.; Bao, Z.; Chen, Y. Evaluation of Solution-Processed Reduced Graphene Oxide Films as Transparent Conductors. *ACS Nano* **2008**, *2*, 463–470.
31. Liu, J.; McCullough, R. D. End Group Modification of Regioregular Polythiophene through Postpolymerization Functionalization. *Macromolecules* **2002**, *35*, 9882–9889.
32. http://www.cem.msu.edu/~reusch/VirtualText/alcohol1.htm
33. Paredes, J. I.; Villar-Rodil, S.; Martinez-Alonson, A.; TascÓn, J. M. D. Graphene Oxide Dispersions in Organic Solvents. *Langmuir* **2008**, *24*, 10560–10564.
34. Philip, B.; Xie, J.; Chandrasekhar, A.; Abraham, J.; Varadan, V. K. A Novel Nanocomposite from Multiwalled Carbon Nanotubes Functionalized with a Conducting Polymer. *Smart Mater. Struct.* **2004**, *13*, 295–298.
35. Song, Y. J.; Lee, J.; Jo, W. H. Multi-walled Carbon Nanotubes Covalently Attached with Poly(3-hexylthiophene) for Enhancement of Field-effect Mobility of Poly(3-hexylthiophene)/Multi-walled Carbon Nanotube Composites. *Carbon* **2010**, *48*, 389–395.
36. Kuila, B. K.; Malik, S.; Batabyal, S. K.; Nandi, A. K. In-Situ Synthesis of Soluble Poly(3-hexylthiophene)/Multiwalled Carbon Nanotube Composite: Morphology, Structure, and Conductivity. *Macromolecules* **2007**, *40*, 278–287.
37. Peng, Q.; Park, K.; Lin, T.; Durstock, M.; Dai, L. Donor-p-Acceptor Conjugated Copolymers for Photovoltaic Applications: Tuning the Open-Circuit Voltage by

Adjusting the Donor/Acceptor Ratio. *J. Phys. Chem. B* **2008**, *112*, 2801–2808.
38. Liao, L.; Dai, L.; Smith, A.; Durstock, M.; Lu, J.; Ding, J.; Tao, Y. Photovoltaic-active Dithienosilole-containing Polymers. *Macromolecules* **2007**, *40*, 9406–9412.
39. Kim, Y.; Bradley, D. D. C. Bright Red Emission from Single Layer Polymer Light-emitting Devices Based on Blends of Regioregular P3HT and F8BT. *Curr. Appl. Phys* **2005**, *3*, 222–226.
40. Sun, Q. J.; Wang, H. Q.; Yang, C. H.; Li, Y. F. Synthesis and Electroluminescence of Novel Copolymers Containing Crown Ether Spacers. *J. Mater. Chem.* **2003**, *13*, 800–806.
41. Bavastrello, V.; Carrara, S.; Kumar, R. M.; Nicoline, C. Optical and Electrochemical Properties of Poly(o-toluidine) Multiwalled Carbon Nanotubes Composite Langmuir-Schaefer Films. *Langmuir* **2004**, *20*, 969–973.
42. Chu, C.; Yang, H.; Hou, W.; Huang, J.; Li, G. Yang, Yang. Control of the Nanoscale Crystallinity and Phase Separation in Polymer Solar cells. *Appl. Phys. Lett.* **2008**, *92*, 103306.